Journal of Geophysical Research: Solid Earth

Supporting Information for

Mechanisms of shear band formation in heterogeneous materials under compression: The role of pre-existing mechanical flaws

Manaska Mukhopadhyay, Arnab Roy and Nibir Mandal*

High Pressure and Temperature Laboratory, Department of Geological Sciences, Jadavpur University, Kolkata 700032, India.

Contents of this file

S1. Comparison of physical properties between Polystyrene and Granite at 500°C

A range of materials, such as synthetic granular solids, polymers and metals have been used as rock analogues to study crustal deformations in laboratory. For example, recent experiments used GRAM (a polymeric rock analogue) to investigate the development of shear bands under compression (Chemenda & Mas, 2016). We chose polystyrene, a commercial available polymer in our experiments. Interestingly, this material displayed deformation localization behaviour, as shown from GRAM. The following sections present a rheological comparison of polystyrene with common crustal rocks.

Yield point versus Young's modulus ratio:

The PS was chosen as an effective rock analogue material based on the rheological equivalence, as required in this kind of experiments. To demonstrate this, we compared the stress versus strain relations of PS with that of granite, which commonly represent the crust. Yield point is one of the most fundamental property of a rock that defines the critical stress at which it plastically yields to deform permanently. Similarly, Young's modulus, the measure of stiffness of an elastic material, is another crucial physical property to determine the pre-yield elastic deformation. To establish our choice of PS as the rock analogue material, we calculated the ratio between yield point and the young's modulus of our material and compared with some classical experimental data given by previous workers (Table S1). As we are considering a depth of upper-mid crustal rocks, we took the yield behaviour of granite at 500°C as our reference.

Author	**Yield Point : Young's Modulus**
Griggs et al., 1960	0.025
Tulis and Yund, 1977	0.027
Jaeger and Cook, 1979 & Ranalli, 1995	0.033
Our Model Material (PS)	*0.035*

Table S1: Comparison of yield point : young's modulus of granite with polystyrene

Poissons' Ratio:

Similar to yield point and young's modulus, Poisson's ratio is another important parameter that governs the elastic property of a material. To establish our choice of polystyrene as model material, we have compared the Poisson's ratio of commonly found upper-mid crustal rocks with Polystyrene (Table S2).

Material type	**Poisson's Ratio**
Granite	0.2-0.3
Marble	0.2-0.3
Quartzite	0.23
Polysterene	*0.34*

Table S2: Comparison of Poisson's ratio of crustal rocks with polystyrene

Dihedral Angle of Shear Bands:

Griggs et al. (1960) showed deformation of rocks at 500°C to 800°C. In their study, they showed shear bands developing in granite at high temperature (in the plastic creep regime)

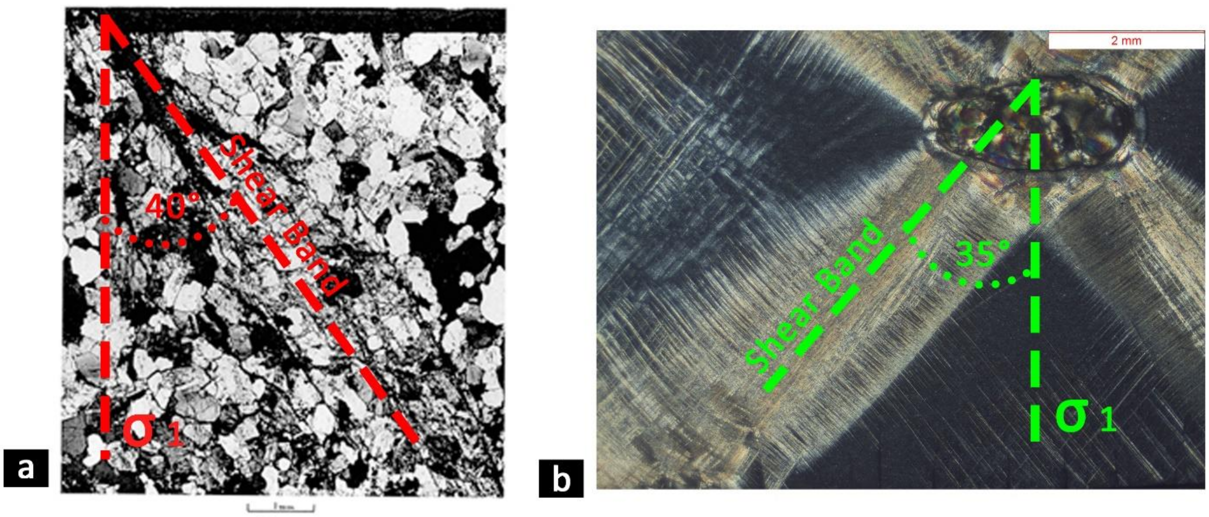

Fig. S1: a) Dihedral angle of granite at high temperature (after *Griggs et al., 1960*); b) Dihedral angle of polystyrene at room temperature

with a dihedral angle of ~80°. This value closely resembles with the dihedral angle of composite bands (~75°) formed in our PS models with heterogeneities, as shown in the Figure S1.

Strain-rate sensitivity

The PS material chosen in the present experiments was sensitive to strain rate, showing a spectacular transition in the mode of shear localization (homogeneous to composite band formation) on a small range ($2x10^{-5}$ s^{-1} to $3x10^{-5}$ s^{-1}) of strain-rate variation in laboratory. We thus varied the strain rate in this narrow range in our experiments with heterogeneous PS models. Previous experimental studies (e.g., Bowden and Raha, 1970) also suggest that the mechanisms (micro- versus diffuse) of shear band formation can transform at some threshold strain rates. This strain-rate sensitivity of PS allows us to explore the effect of strain rate variations in geological conditions, e.g., 10^{-12} s^{-1} to 10^{-14} s^{-1}, as commonly reported in literature (Fagereng & Biggs, 2019; Pfiffner & Ramsay, 1982).

S2. Birefringence in deformed polymers

PS in its completely amorphous state is characterized by randomly oriented polymer molecular chains, and shows optically isotropic behavior (Fig. S2). The material

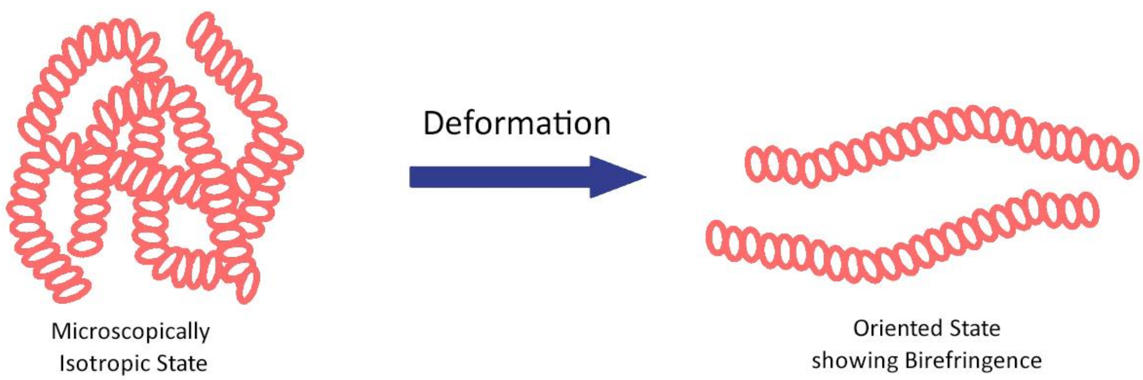

Fig. S2: a) Schematic diagram showing generation of birefringence due to deformation in polymers (after *Tagaya, 2013*).

in an undeformed condition is thus devoid of any birefringence. However, under stressed conditions, the randomly oriented polymer chains are aligned in a preferred direction, and such directionality in chain structures gives rise to anisotropic properties, as reflected in optical birefringence (Tagaya, 2013). The magnitude of birefringence holds a good correlation with the amount of plastic strain accumulation that determines the degree of molecular chain orientations. The deformation induced birefringence is irreversible as it develops in response to permanent strains in the material. We could thus qualitatively use this birefringence property to delineate the zones of permanent strain localization in deformed PS blocks.

S3. Homogeneous model experiments at lower strain rate

We performed an additional set of experiments to test the sensitivity of homogenous PS blocks to strain rate in forming shear band structures (Fig. S3). The experiments were run at a lower strain rate, 3 x 10^{-5} s^{-1} to 2 x 10^{-5} s^{-1}, as compared to those presented in the main text (Fig. 3a). This range of strain rates produced sharp and narrow bands that are finely spaced and uniformly distributed in the entire model. They typically formed in conjugate sets, symmetrically oriented with respect to the compression direction. The bands multiplied in number with increasing finite strain, as observed in similar

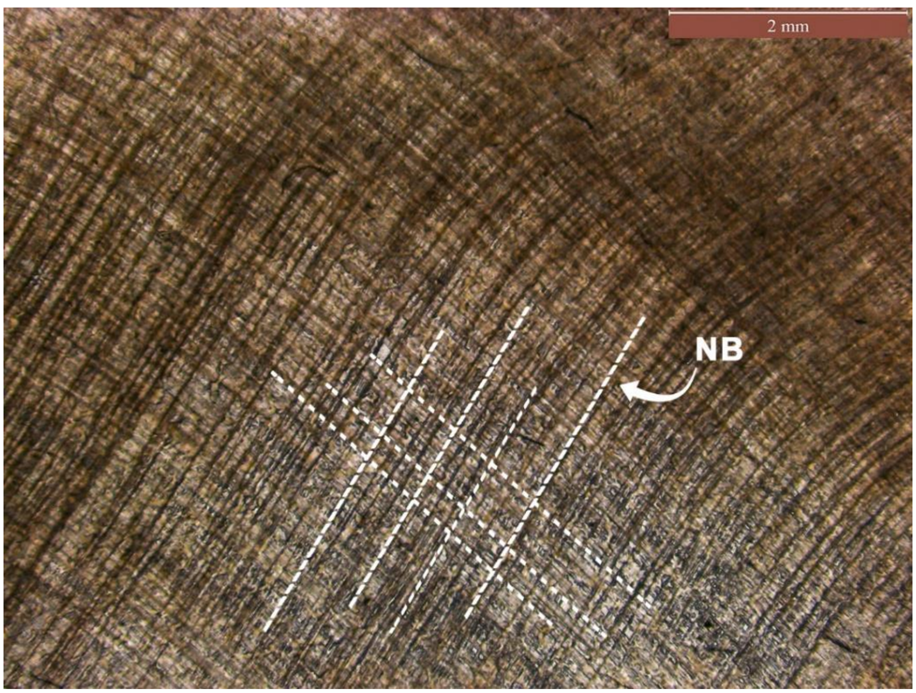

Fig. S3: Uniform development of closely spaced, conjugate narrow bands in homogenous PS models deformed at low strain rate ($\dot{\varepsilon} = 2 \text{ x } 10^{-5}\ s^{-1}$). Note that strain rate doesn't have any effect on shear band formation in homogeneous model.

experiments at relatively higher rates, and they had no tendency to widen, but grow in length. The PS produced distributed narrow bands in its homogeneous state under the entire range of strain rate conditions used in our laboratory experiments. We thus conclude that uniformly thick bands of homogeneous shear in low-strain rate experiments reflect the influence of weak flaws in the model.

S4. Experimental result of heterogeneous model with a single hole

An additional set of compression experiments was performed on polystyrene blocks containing single flaws in the middle of the model. The flaw diameter was kept 1mm, similar to the experiments with multiple flaws. The experiments were conducted at room temperature under strain rates similar to the previous ones. The single-flaw models

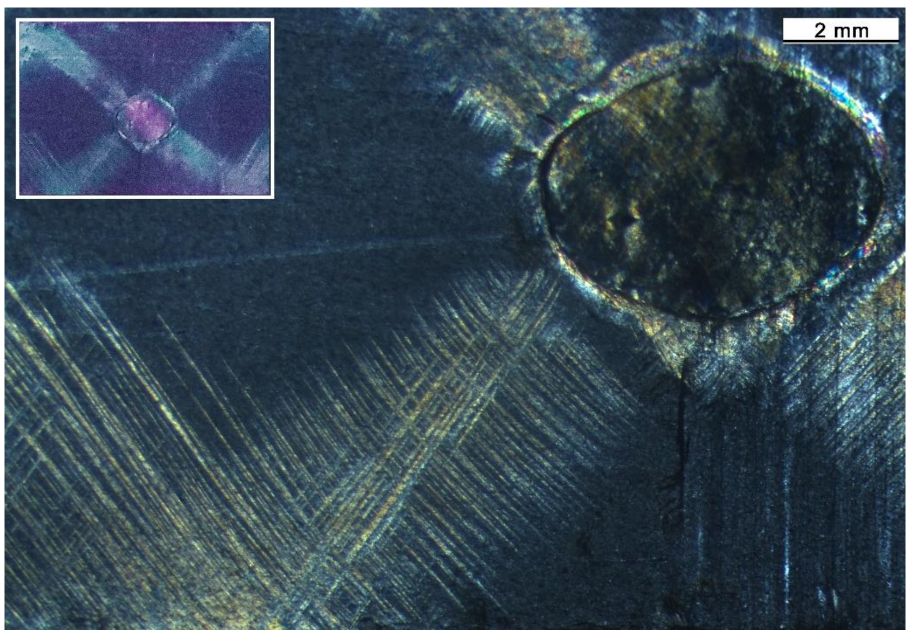

Fig S4: Development of shear band patterns in a single-flaw polystyrene model. The full view of bands around the flaw is shown in the inset. Note that the composite band geometry and its internal band structure are identical to that produced in a model containing a pair of flaws. The single-flaw experiments confirm that there were no mutual interactions between flaws in the experiments presented in the main text.

produced a pattern exactly similar to those observed in experiments containing two flaws (Fig. S4). The single-flaw experiments clearly reveal the absence of any mutual interaction between the flaws in the two-flaw experiments. The weak heterogeneities considered in our experimental modelling acted as a single mechanical entity in the mechanics of shear band localization.

S5. Calculation of finite strain

Let $\acute{\alpha}$, $\acute{\beta}$, be the angle formed by the passive marker with shear zone and shear band boundary respectively. Also, $2y_1$ and $2y_2$ are the shear zone and shear band thickness

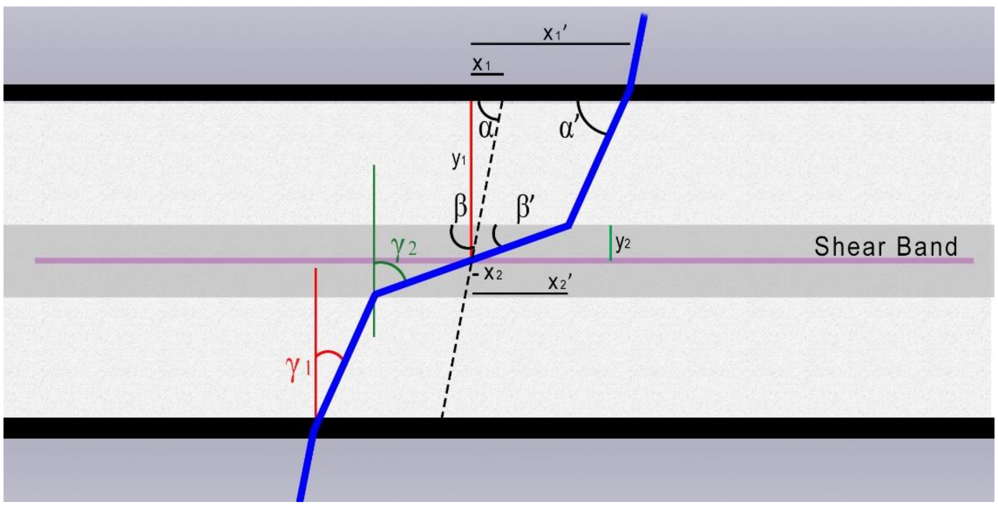

Fig. S5: Schematic representation of finite strain measurement using a passive marker (blue line).

respectively. Let γ be the total finite strain. We know that,

$$\gamma = \gamma_1 + \gamma_2 \quad \text{(S1)}$$

From Fig S5,

$$\acute{x}_1 = x_1 + \gamma_1 y_1 \quad \text{(S2)}$$

Dividing both side by y, we get

$$\frac{\acute{x}_1}{y_1} = \frac{x_1}{y_1} + \gamma_1 \quad \text{(S3)}$$

$$\cot \acute{\alpha} = \cot \alpha + \gamma_1 \quad \text{(S4)}$$

Similarly, from Fig. S5,

$$\frac{\acute{x}_2}{y_2} = \frac{x_2}{y_2} + \gamma_2 \quad \text{(S5)}$$

$$\cot \acute{\beta} = \cot \beta + \gamma_2 \qquad \text{(S6)}$$

We calculate the total finite strain using Eq. S1.

S6. Mesh refinement study

We performed a mesh refinement test to evaluate the sensitivity of band structures with varying mesh resolution sensitivity in our elasto-visco-plastic numerical models. The

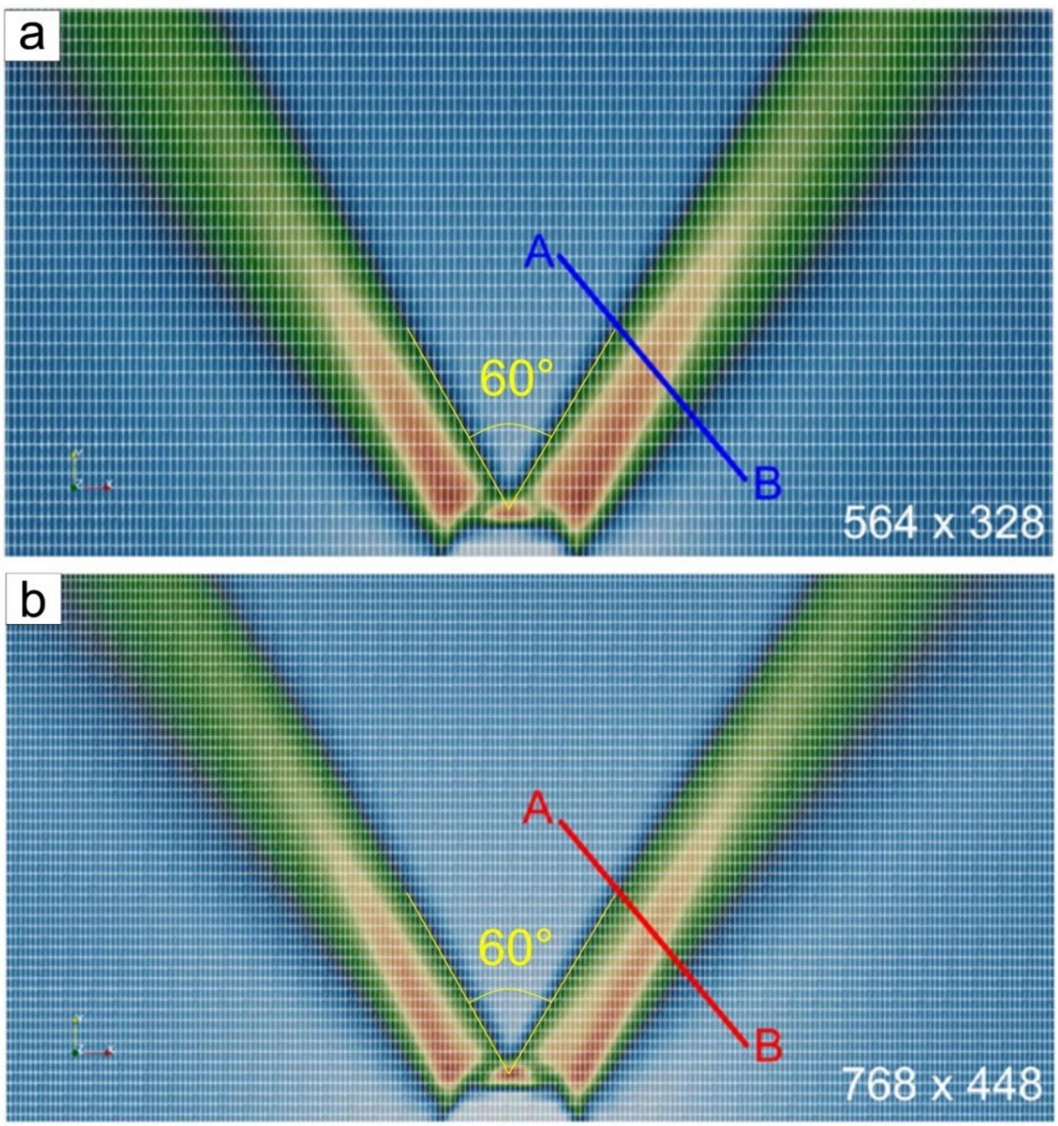

Fig. S6.1: Two numerical simulations run under the same conditions, but with different mesh resolution: a) 564x328 b) 768x448.

test revealed that the band structures hardly changed after attaining a fine resolution. For example, two simulations run under exactly the same conditions but with different mesh resolutions, 768x448 and 564x384, produce almost identical shear band structures with minute details (Fig. S6.1). The mesh resolution of 564x384 was thus chosen for all the simulation runs presented in this study. Earlier workers have also used the mesh resolution of the same order in their simulations (Duretz et al., 2019).

The two experiments show similar dihedral angle between the shear bands (60°) and similar pattern of the magnitude of accumulated strain along the profile AB (Fig. S6.2) across the shear bands.

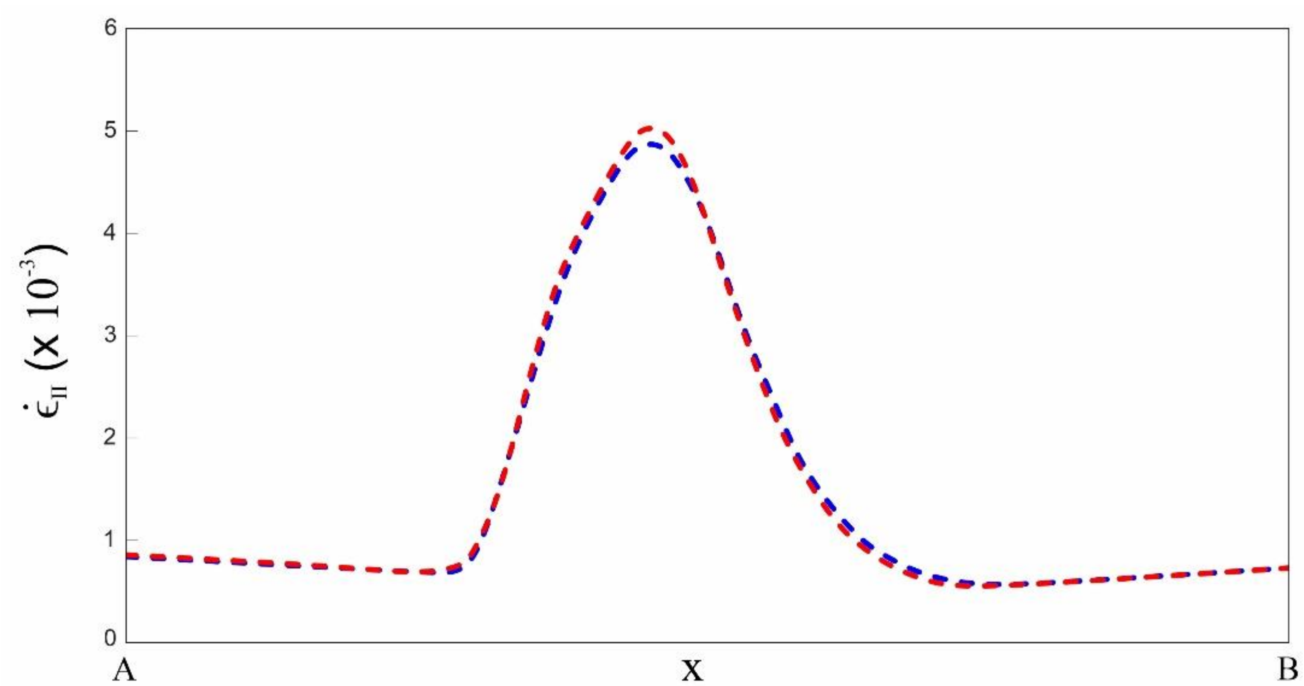

Fig S6.2: Profiles of accumulated strain probed across the shear bands of two different set of numerical simulation with resolution 564x328 (blue line) and 768x448 (red line).

S7. Across-band strain profiles in numerical models

This section discusses the strain profiles calculated from the numerical simulation MS2 run at relatively high rates (results presented in the main text). The profiles are constructed along the lines AB, CD, EF, as shown in Figure 6 in the main text. They represent plots of the 2nd invariant of the strain rate tensor (sum of the elastic, viscous and plastic strain components) as a function of distance in the model. The strain profiles contain multiple peaks that reveal the composite nature of shear bands, as observed in the PS experiments at a high strain rate (3 x 10^{-5} s^{-1}).

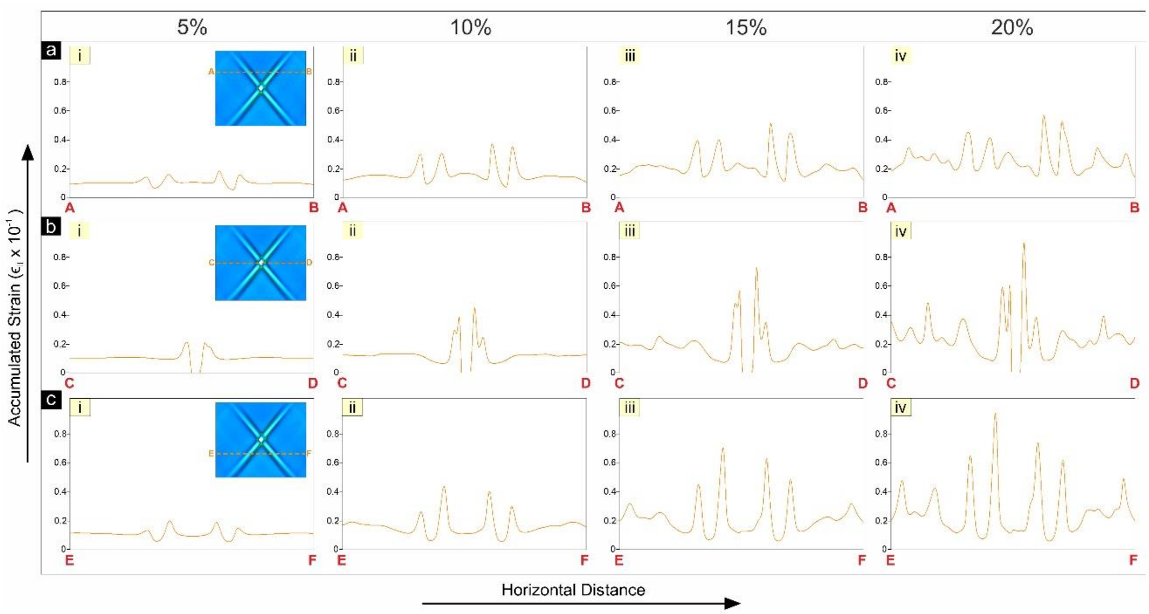

Fig S7: Across-band strain profiles in MS2 (locations of the profile lines: AB, CD, and EF, shown in inset). Note that the strain profiles show multiple peaks signifying the formation of multiple shear bands in the core zone.

S8. Field study of natural shear zones

We studied a few centimetres to tens of metres long ductile shear zones in the Chotanagpur Granite Gneissic Complex (CGGC), focusing upon regions north of the South Purulia Shear Zone (SPSZ). The shear zones are associated with alkali granite, brecciated quartzite, apatite-magnetite bearing chert, U-Th mineral-bearing pegmatite and mafic-ultramafic rocks. The host rock types include banded, porphyritic and augen granite gneisses, garnet-bearing quartzo-feldspathic gneisses, khondalite, amphibolites and mafic granulites, which generally contain penetrative tectonic foliations of single or multiple generations. The host foliations act as markers, showing sharp deflections across shear bands that allow us to identify the mode of shear localization. In places we could recognize mechanical heterogeneities as nucleating agents of shear zones. For example, high-temperature metamorphic rocks in the Jasidh area show band localization in the vicinity of quartzo-feldspathic aggregates, which possibly represent melt lenses (weak zones) produced by partial melting during the granulite facies metamorphism. This kind of field examples support our experimental interpretation that mechanically weak heterogeneities can be a crucial factor for the formation of isolated shear zones in continua.

We chose three prominent locations: 1) Bero Hillocks (23°32'09.5" N, 86°40'01.3" E) near Raghunathpur town, 2) Purulia-Asansol Road transect near Baraseni (23°25'20.9"N 86°28'48.8"E), and 3) Jasidih (24° 31′ 19.2″ N, 86° 38′ 51.72″ E) (Fig S8). Location 1 is predominantly composed of biotitic granite gneiss, which shows excellent shear band structures with thick strongly shear core, sometimes flanked by excellent drag zones on both sides, while some shows relatively weakly deformed matrix. Lithologically, Location 2 is a fine-grained granulite-facies rock, primarily composed of alkali-feldspar, with minor amounts of quartz, mica, garnet and tourmaline. Classically this rock type is also termed as Leptynite and they often show a planar gneissic structure. Location 2 exhibits extensive micro shear band structures with a cross cutting relationship throughout the exposure (Fig. 8 a). Location 3 is situated near the Jasidih area, which lies in the northernmost part of CGGC. Lithologically, this area is predominantly of migmatitic felsic orthogneiss origin, with random enclaves of meta -sedimentary and meta-mafic rocks. We found excellent shear bands occurring in the vicinity of elliptical to semi-elliptical heterogenous clasts (Fig 8b), that can be well correlated with our heterogenous models (Fig. 3 b).

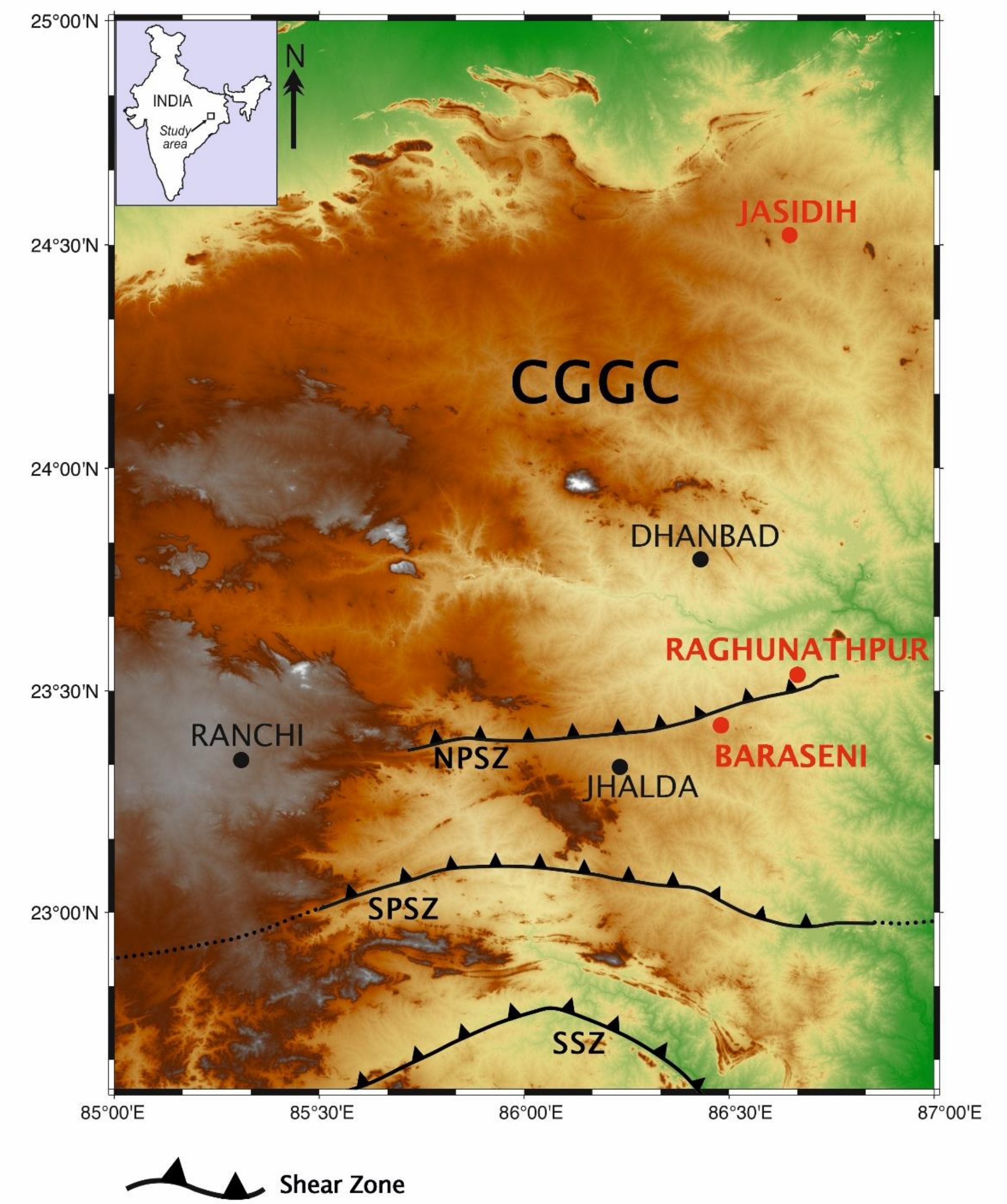

Fig. S8: A simplified geological map of the East Indian Precambrian craton, showing the locations of the Singhbhum Shear Zone (SSZ), the South Purulia Shear Zone (SPSZ), the North Purulia Shear Zone (NPSZ) and the Chotanagpur Granite Gniess Complex (CGGC). Field areas are marked by red dots in the map.

S9. Strain profiles from field studies

This section presents the strain profiles obtained from strain analyses performed in field outcrops. Strain profiles were obtained by calculating the finite strain (ε) across various types of shear zones. Type I shear zones containing narrow shear bands observed in an area near Purulia town, showed a characteristic curve with a high peak showing large ε values implying intense shear localisation across the narrow shear bands (Fig 9b-i). Type II shear zones showed gradational shear strain variation from weakly deformed wall to highly sheared core forming a typical bell-shaped curve (Fig 9b-ii). On the contrary, Type III shear zones are characterized by a plateau like strain profile with very narrow gradational zone (Fig 9b-iii). This characteristic shape results due to formation of a very narrow drag zone on both sides of the homogenous core zone.

References:

Chemenda, A. I., & Mas, D. (2016). Dependence of rock properties on the Lode angle: Experimental data, constitutive model, and bifurcation analysis. *Journal of the Mechanics and Physics of Solids*, *96*, 477–496. https://doi.org/10.1016/j.jmps.2016.08.004

Duretz, T., de Borst, R., & Le Pourhiet, L. (2019). Finite Thickness of Shear Bands in Frictional Viscoplasticity and Implications for Lithosphere Dynamics. *Geochemistry, Geophysics, Geosystems*, *20*(11), 5598–5616. https://doi.org/10.1029/2019GC008531

Fagereng, Å., & Biggs, J. (2019). New perspectives on ‘geological strain rates’ calculated from both naturally deformed and actively deforming rocks. *Journal of Structural Geology*, *125*(October 2018), 100–110. https://doi.org/10.1016/j.jsg.2018.10.004

Pfiffner, O. a, & Ramsay, J. G. (1982). Conventional Strain. *Journal of Geophysical Research B: Solid Earth*, *87*(B1), 311–321.

Tagaya, A. (2013). Encyclopedia of Polymeric Nanomaterials. *Encyclopedia of Polymeric Nanomaterials*, 1–6. https://doi.org/10.1007/978-3-642-36199-9